

## Article

# Study on Magnetic and Plasmonic Properties of Fe<sub>3</sub>O<sub>4</sub>-PEI-Au and Fe<sub>3</sub>O<sub>4</sub>-PEI-Ag Nanoparticles

Shuya Ning<sup>1,2</sup>, Shuo Wang<sup>1</sup>, Zhihui Liu<sup>1</sup>, Naming Zhang<sup>3,\*</sup>, Bin Yang<sup>3</sup> and Fanghui Zhang<sup>1</sup>

<sup>1</sup> School of Electronic Information and Artificial Intelligence, Shaanxi University of Science and Technology, Xi'an 710021, China; ningshuya@sust.edu.cn (S.N.); wangshuo.99@sust.edu.cn (S.W.); lewis\_zhihui@sust.edu.cn (Z.L.); zhangfanghui@sust.edu.cn (F.Z.)

<sup>2</sup> Key Laboratory of Photonics Technology for Information, School of Electronic and Information Engineering, Xi'an Jiaotong University, Xi'an 710049, China

<sup>3</sup> State Key Laboratory of Electrical Insulation and Power Equipment, School of Electrical Engineering, Xi'an Jiaotong University, Xi'an 710049, China; yangbin.2008@stu.xjtu.edu.cn

\* Correspondence: namingzhang@xjtu.edu.cn

**Abstract:** Magnetic–plasmonic nanoparticles (NPs) have attracted great interest in many fields because they can exhibit more physical and chemical properties than individual magnetic or plasmonic NPs. In this work, we synthesized Au- or Ag-decorated Fe<sub>3</sub>O<sub>4</sub> nanoparticles coated with PEI (Fe<sub>3</sub>O<sub>4</sub>-PEI-M (M = Au or Ag) NPs) using a simple method. The influences of the plasmonic metal NPs' (Au or Ag) coating density on the magnetic and plasmonic properties of the Fe<sub>3</sub>O<sub>4</sub>-PEI-M (M = Au or Ag) NPs were investigated, and the density of the plasmonic metal NPs coated on the Fe<sub>3</sub>O<sub>4</sub> NPs surfaces could be adjusted by controlling the polyethyleneimine (PEI) concentration. It showed that the Fe<sub>3</sub>O<sub>4</sub>-PEI-M (M = Au or Ag) NPs exhibited both magnetic and plasmonic properties. When the PEI concentration increased from 5 to 35 mg/mL, the coating density of the Au or Ag NPs on the Fe<sub>3</sub>O<sub>4</sub> NPs surfaces increased, the corresponding magnetic intensity became weaker, and the plasmonic intensity was stronger. At the same time, the plasmonic resonance peak of the Fe<sub>3</sub>O<sub>4</sub>-PEI-M (M = Au or Ag) NPs was red shifted. Therefore, there was an optimal coverage of the plasmonic metal NPs on the Fe<sub>3</sub>O<sub>4</sub> NPs surfaces to balance the magnetic and plasmonic properties when the PEI concentration was between 15 and 25 mg/mL. This result can guide the application of the Fe<sub>3</sub>O<sub>4</sub>-M (M = Au or Ag) NPs in the biomedical field.

**Keywords:** Fe<sub>3</sub>O<sub>4</sub>-PEI-M (M = Au or Ag) nanoparticles; plasmonic; magnetic



**Citation:** Ning, S.; Wang, S.; Liu, Z.; Zhang, N.; Yang, B.; Zhang, F. Study on Magnetic and Plasmonic Properties of Fe<sub>3</sub>O<sub>4</sub>-PEI-Au and Fe<sub>3</sub>O<sub>4</sub>-PEI-Ag Nanoparticles. *Materials* **2024**, *17*, 509. <https://doi.org/10.3390/ma17020509>

Academic Editors: Aivaras Kareiva and Bryan M. Wong

Received: 10 December 2023

Revised: 17 January 2024

Accepted: 18 January 2024

Published: 21 January 2024



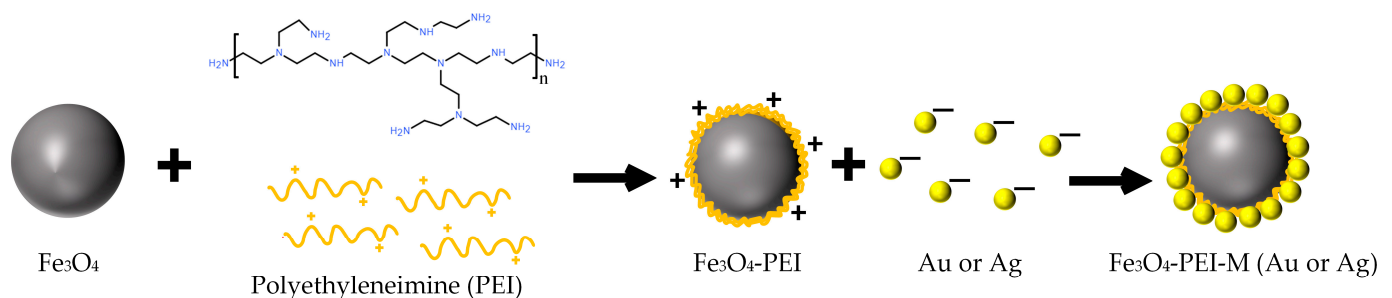
**Copyright:** © 2024 by the authors. Licensee MDPI, Basel, Switzerland. This article is an open access article distributed under the terms and conditions of the Creative Commons Attribution (CC BY) license (<https://creativecommons.org/licenses/by/4.0/>).

## 1. Introduction

At present, magnetic nanoparticles (NPs) have attracted great interest in many fields, such as bearing drugs [1,2], radionuclides [3,4], hyperthermia [5–7], active magnetic field targeting [8–10], protein purification [11–13], biosensors [14,15], and catalysis [16–18]. Researchers also further modify the surface of magnetic NPs with antibodies or proteins to expand their applications [19–21]. As such, Sohn et al. combined iron oxide nanoparticles with glucose transporter 1 antibody for vascular therapy [19]. Gawali et al. prepared magnetic nanoparticles conjugated with bovine serum albumin protein for magnetothermal therapy [21]. Unfortunately, magnetic NPs can easily aggregate, and it is difficult for them to couple with biomolecules due to the lack of functional groups, which limits the applications of magnetic nanomaterials [22]. In order to overcome these shortcomings, metal or metal oxide shells were coated on the surface of the magnetic nanomaterials to decorate the nanoparticles [23]. Noble metals (Au, Ag) are considered to be the most ideal coating material due to their unique optical properties, localized surface plasmon resonance (LSPR), high stability, biocompatibility, and easy surface functionalization [24–27]. Magnetic–plasmonic NPs, consisting of plasmonic metal materials (Au or Ag) coated onto

the surfaces of magnetic NPs, can exhibit more physical and chemical properties than individual magnetic or plasmonic NPs, such as magnetic, plasmonic, biological, compatibility, chemical stability, and physicochemical properties [28–31]. They are considered as effective candidate materials for catalysts [32], sensors [33], antibacterial materials [34], cancer detection [35], and medical applications [36]. Therefore, it is of great significance to combine magnetic NPs with noble metal materials to generate nanoparticles that simultaneously exhibit both excellent magnetic and plasmonic characteristics. This has been the focus of many researchers in recent years. In 2020, Kou et al. prepared flower-shaped  $\text{Fe}_3\text{O}_4$ -Au NPs and found that the magnetic properties gradually decreased by increasing the amount of Au seeds [37]. Aarathi et al. synthesized  $\text{Fe}_3\text{O}_4/\text{Ag}$  NPs and studied the surface-enhanced Raman scattering (SERS), and the photocatalytic and antibacterial activities of the nanoparticles [38]. Oguzlar studied  $\text{Fe}_3\text{O}_4$  and  $\text{Fe}_3\text{O}_4/\text{Ag}$  NPs to improve the oxygen sensitivity of ruthenium dyes [39]. In 2021, Du et al. synthesized  $\text{Fe}_3\text{O}_4/\text{Au}$  core-shell NPs and studied both the magnetic and optical properties derived from the  $\text{Fe}_3\text{O}_4$  NPs and the Au nano-shells [40]. Salimi et al. prepared Au- $\text{Fe}_3\text{O}_4$  NPs and studied the nano-morphology and formation process of the Au- $\text{Fe}_3\text{O}_4$  NPs [41]. In 2022, Lv et al. prepared the  $\text{Fe}_3\text{O}_4/\text{Au}$  NPs, which showed LSPR absorption in the near-infrared region [42]. Mikoliunaite et al. prepared  $\text{Fe}_3\text{O}_4/\text{Ag}$  NPs and found that their plasmonic resonance could be varied from 470 to 800 nm by changing the volume of the Ag colloid solution [43]. In 2023, Ravichandran et al. synthesized  $\text{Fe}_3\text{O}_4/\text{Ag}$  NPs and studied the dye removal rate of the  $\text{Fe}_3\text{O}_4/\text{Ag}$  NPs in the presence of a reducing agent [44]. According to the above works, most of the research on  $\text{Fe}_3\text{O}_4$ -M (M = Au or Ag) NPs was limited to a single particle type or physical property, and studies on the relationships between the coverage of the plasmonic metal NPs on the magnetic NPs surfaces and both the magnetic and plasmonic properties are lacking. Therefore, it is important to systematically investigate the magnetic and plasmonic characteristics of  $\text{Fe}_3\text{O}_4$ -M (M = Au or Ag) NPs.

In this work, we prepared the Au- or Ag-decorated  $\text{Fe}_3\text{O}_4$  nanoparticles coated with PEI ( $\text{Fe}_3\text{O}_4$ -PEI-M (M = Au or Ag) NPs) using a simple method.  $\text{Fe}_3\text{O}_4$  NPs were synthesized through a co-precipitation method, and plasmonic metal (Au or Ag) NPs were prepared using a chemical reduction method.  $\text{Fe}_3\text{O}_4$  NPs and plasmonic metal NPs were mixed at room temperature to form  $\text{Fe}_3\text{O}_4$ -PEI-M (M = Au or Ag) NPs. In this process, positively charged PEI was assembled onto negatively charged  $\text{Fe}_3\text{O}_4$  through electrostatic self-assembly. Then, negatively charged plasmonic metal NPs were electrostatically bound to the positively charged PEI-coated  $\text{Fe}_3\text{O}_4$  NPs, resulting in a formation of  $\text{Fe}_3\text{O}_4$ -PEI-M (M = Au or Ag) NPs (Scheme 1). The density of the plasmonic metal NPs coated on the  $\text{Fe}_3\text{O}_4$  NPs was adjusted by controlling the concentration of polyethyleneimine (PEI), and the effects of the plasmonic metal NPs' density on the magnetic and plasmonic properties of the  $\text{Fe}_3\text{O}_4$ -PEI-M (M=Au or Ag) NPs were studied. The relationships between the coating density of the plasmonic metal NPs and both the magnetic and plasmonic properties were established. This work can provide guidance for the application of  $\text{Fe}_3\text{O}_4$ -M (M = Au or Ag) NPs in the biomedical field.



**Scheme 1.** Schematic of the preparation of  $\text{Fe}_3\text{O}_4$ -PEI-M (M = Au or Ag) nanoparticles.

## 2. Materials and Methods

### 2.1. Materials

Ferric chloride hexahydrate ( $\text{FeCl}_3 \cdot 6\text{H}_2\text{O}$ ), ferrous chloride tetrahydrate ( $\text{FeCl}_2 \cdot 4\text{H}_2\text{O}$ ), and ammonium hydroxide (28–30%  $\text{NH}_3$ ) were obtained from Merck (Shanghai, China). Polyethyleneimine (PEI, branched,  $M_w \approx 10,000$  g/mol), sodium hydroxide (NaOH), chloroauric acid ( $\text{HAuCl}_4$ ), silver nitrate ( $\text{AgNO}_3$ ), sodium borohydride ( $\text{NaBH}_4$ ), and sodium citrate ( $\text{C}_6\text{H}_5\text{Na}_3\text{O}_7 \cdot 2\text{H}_2\text{O}$ ) were obtained from Aladdin (Shanghai, China). All chemicals were used as received with no further purification.

### 2.2. Synthesis of $\text{Fe}_3\text{O}_4$ Nanoparticles

$\text{Fe}_3\text{O}_4$  nanoparticles were synthesized through a co-precipitation method [45]. A total of 4.25 g of  $\text{FeCl}_3 \cdot 6\text{H}_2\text{O}$  and 2 g of  $\text{FeCl}_2 \cdot 4\text{H}_2\text{O}$  were added to 200 mL of ultrapure water. In an oxygen-free environment, the mixture was heated to 70 °C with stirring at 800 rpm and maintained at this temperature for 1 h. A total of 10 mL of ammonia solution (25% wt) was added into the mixture. A black precipitate was produced, indicating the formation of  $\text{Fe}_3\text{O}_4$  NPs. The resulting solution was stirred for another 15 min. The nanoparticles were purified by means of magnetic separation five times and then redispersed in 200 mL of ultrapure water for further use.

### 2.3. Synthesis of Au Nanoparticles

Au nanoparticles were synthesized through  $\text{NaBH}_4$  reduction of chloroauric acid [29]. Firstly, 0.5 mL of 0.01 M  $\text{HAuCl}_4$  was mixed with 0.5 mL of a 0.01 M trisodium citrate solution. Then, the mixture was added into 18 mL of ultrapure water and stirred at 1200 rpm. A total of 0.5 mL of an ice 0.04 M  $\text{NaBH}_4$  solution was quickly added with vigorous stirring at room temperature. When the solution turned pink, indicating the formation of Au NPs, the solution was allowed to stand for 2 h. The particles were collected by centrifugation at 14,000 rpm for 10 min. The Au nanoparticles were stored in the fridge until further use.

### 2.4. Synthesis of Ag Nanoparticles

Ag nanoparticles were prepared through the  $\text{NaBH}_4$  reduction of silver nitrate [46]. Briefly, 10 mL of a 1 mM  $\text{AgNO}_3$  solution was mixed with 0.8 mL of 40 mM sodium citrate solution used as stabilizer. A total of 0.2 mL of an ice 0.06 M  $\text{NaBH}_4$  solution was added into the mixture, and the mixture was stirred at 1200 rpm for 15 min. After the solution turned dark yellow, indicating the formation of Ag NPs, the Ag nanoparticles were collected by means of centrifugation at 14,000 rpm for 10 min. The Ag nanoparticles were stored in the fridge until further use.

### 2.5. Synthesis of $\text{Fe}_3\text{O}_4$ -PEI-M (M = Au or Ag) NPs

Firstly, 2 mL of the  $\text{Fe}_3\text{O}_4$  NPs suspension (1 mg/mL) was mixed with 20 mL of the PEI solution. After 60 min of ultrasonic treatment, the mixture was left to stand for half an hour [47]. Subsequently, magnetic separation was employed for washing the nanoparticles. The PEI-coated  $\text{Fe}_3\text{O}_4$  NPs were finally redispersed in 2 mL of ultrapure water. Then, the 0.5 mL PEI-coated  $\text{Fe}_3\text{O}_4$  NPs solution was mixed with 4.5 mL of the plasmonic metal (Au or Ag) NPs solution. The mixture was continuously stirred at 2000 rpm for 45 min. Finally, the Au- or Ag-decorated  $\text{Fe}_3\text{O}_4$  nanoparticles coated with PEI were collected by magnetic separation and washed with ultrapure water three times. By varying the concentrations of the PEI solution, the adhesion density of the plasmonic metal NPs on the  $\text{Fe}_3\text{O}_4$  NPs surfaces could be changed.

### 2.6. Electric Field Simulation

To investigate the plasmonic properties of nanoparticles, the electric field distributions of the nanoparticles were simulated using the finite element method with the commercial software COMSOL 5.5. The excitation beam was a plane wave polarized along the x-axis

with the plasmonic resonance wavelength of the nanoparticle, and the permittivities of Au and Ag were taken from the experimental data of Johnson and Christy [48]. The mesh size was set to 2 nm.

### 2.7. Characterization

The morphology and structure of the nanoparticles were observed by scanning electron microscopy (SEM, JSM-7000F, JEOL, Tokyo, Japan) and transmission electron microscopy (TEM, JEM-2100, JEOL, Tokyo, Japan). Hydrodynamic diameter and zeta-potential measurements were carried out using dynamic light scattering (DLS, Delsa, Palmdale, CA, USA). The crystalline structure of the nanoparticles was analyzed by X-ray powder diffraction (XRD, D8 ADVANCE, Bruker, Bremen, Germany). UV-visible absorption spectra were obtained using a UV-vis spectrophotometer (Cary 5000, Agilent, Santa Clara, CA, USA). Magnetization measurements of the nanoparticles were performed using a vibrating sample magnetometer (MPMS-squid VSM-094, Quantum Design, San Diego, CA, USA).

## 3. Results and Discussion

### 3.1. Study on the Plasmonic Metal Nanoparticles

#### 3.1.1. Au Nanoparticles

To prepare suitable Au nanoparticles for coating Fe<sub>3</sub>O<sub>4</sub> NPs' surfaces, we investigated the influence of the reducing agent (NaBH<sub>4</sub>) concentrations on the Au nanoparticles. Figure 1 shows the SEM images of the Au NPs synthesized with NaBH<sub>4</sub> concentrations ranging from 4 to 0.04 M. We found that the synthesized Au nanoparticles formed agglomerates with an average diameter of about 12 nm when the NaBH<sub>4</sub> concentration was 4 M (Figure 1a). With a decrease in the NaBH<sub>4</sub> concentration from 4 to 0.04 M, the Au NPs became more diffuse, and the particle size became more uniform. When the NaBH<sub>4</sub> concentration was 0.04 M, the average diameter of the Au NPs was about 10 nm, as shown in Figure 1f, and there was excellent dispersion, which was beneficial for attachment on the Fe<sub>3</sub>O<sub>4</sub> NPs' surfaces. Figure 1 shows that the particles size increased and more easily agglomerated with the increase in NaBH<sub>4</sub> concentration. This is attributed to the over-reduction of HAuCl<sub>4</sub> in the case of excessive amounts of reducing agent [49,50].

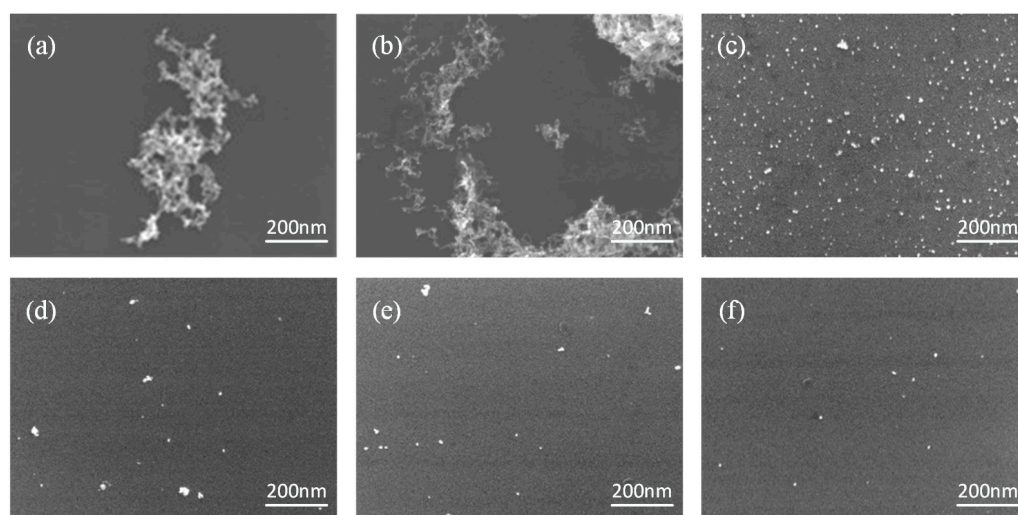


**Figure 1.** SEM images of the Au NPs prepared with (a) 4 M, (b) 2 M, (c) 1 M, (d) 0.4 M, (e) 0.08 M, and (f) 0.04 M NaBH<sub>4</sub> solution.

#### 3.1.2. Ag Nanoparticles

In addition, we also investigated the Ag NPs, which were prepared using trisodium citrate as a stabilizer and NaBH<sub>4</sub> to reduce AgNO<sub>3</sub>. Figure 2 shows the SEM images of the Ag NPs prepared with different NaBH<sub>4</sub> concentrations. We found that the synthesized

Ag nanoparticles formed agglomerates with an average diameter of about 25 nm when the  $\text{NaBH}_4$  concentration was 8.5 M (Figure 2a). With a decrease in the  $\text{NaBH}_4$  concentration from 8.5 to 0.06 M, the Ag NPs became more diffuse, and the size became more uniform [51]. This was due to more Ag atoms being produced with the increase in  $\text{NaBH}_4$  concentration [49]. When the concentration of  $\text{NaBH}_4$  was 0.06 M, the average diameter of the Au NPs was about 10 nm, as shown in Figure 2f, and there was excellent dispersion, which is desirable for the further preparation of Ag-decorated  $\text{Fe}_3\text{O}_4$  NPs.

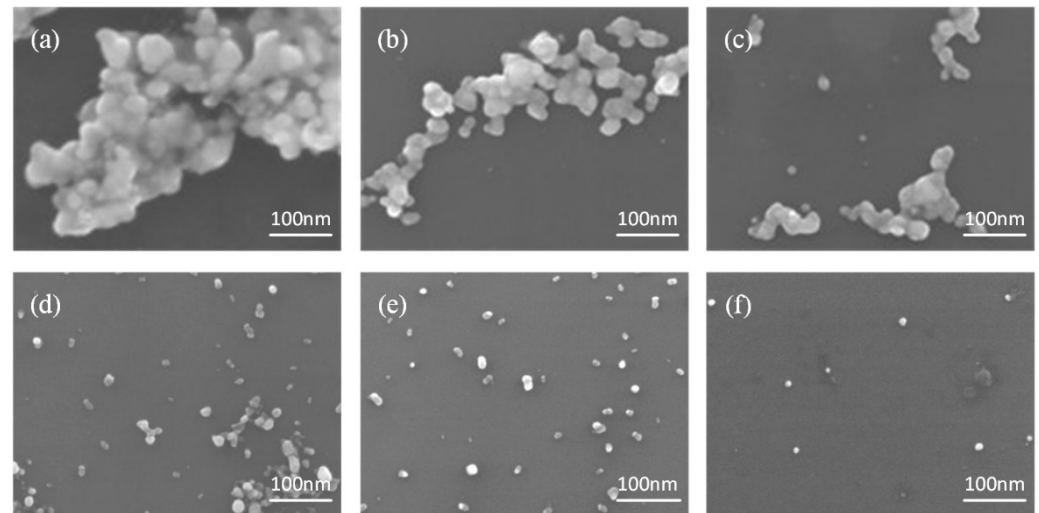


**Figure 2.** SEM images of the Ag NPs prepared with (a) 8.5 M, (b) 0.85 M, (c) 0.43 M, (d) 0.17 M, (e) 0.08 M, and (f) 0.06 M  $\text{NaBH}_4$  solution.

### 3.2. Study on the Properties of the $\text{Fe}_3\text{O}_4$ -PEI-Au Nanoparticles

#### 3.2.1. $\text{Fe}_3\text{O}_4$ -PEI-Au Nanoparticles

In order to explore the magnetic and plasmonic properties of the Au-decorated  $\text{Fe}_3\text{O}_4$  nanoparticles, we synthesized the  $\text{Fe}_3\text{O}_4$ -PEI-Au NPs with different densities of Au NPs on the  $\text{Fe}_3\text{O}_4$  NPs surfaces. Figure 3 shows the SEM image of the  $\text{Fe}_3\text{O}_4$  NPs, and the average size was about 80 nm in diameter.

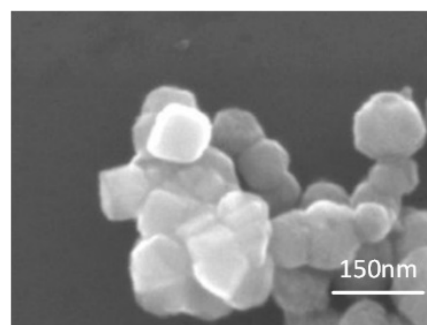


**Figure 3.** SEM image of the  $\text{Fe}_3\text{O}_4$  NPs.

The coating density of Au NPs on the  $\text{Fe}_3\text{O}_4$  NPs surfaces was controlled by changing the PEI concentration. PEI is used as a bonding material. It is a water-soluble cationic polymer which contains amino and imino groups in each polymer chain. When the polymer PEI is dispersed in aqueous solution, each polymer chain is positively charged due to the amino and imino groups [52]. When the  $\text{Fe}_3\text{O}_4$  NPs are immersed in a PEI solution, positively charged PEI is assembled onto the negatively charged  $\text{Fe}_3\text{O}_4$  through electrostatic self-assembly, leading to the formation of a stable polyelectrolyte layer. Subsequently, the negatively charged Au NPs are easily electrostatically bound to the positively charged PEI-coated  $\text{Fe}_3\text{O}_4$  NPs, resulting in a formation of the  $\text{Fe}_3\text{O}_4$ -PEI-Au NPs [53]. Figure 4

shows the SEM and TEM images of the Au-decorated  $\text{Fe}_3\text{O}_4$  NPs treated with different concentrations of PEI solutions. It shows that 10 nm diameter Au NPs were attached to the surfaces of 80 nm diameter  $\text{Fe}_3\text{O}_4$  NPs. DLS measurements depicted that the hydrodynamic diameter of the  $\text{Fe}_3\text{O}_4$ -PEI-Au NPs is about 131 nm (shown in Figure 5), and the zeta potential is around +18.4 mV. When the  $\text{Fe}_3\text{O}_4$  NPs were treated with a 5 mg/mL PEI solution, a small amount of Au NP was coated on the  $\text{Fe}_3\text{O}_4$  NPs' surfaces, as shown in Figure 4a,e. With an increase in the PEI concentration from 5 to 35 mg/mL, the coating density of the Au NPs gradually increased, and thus the coverage of the Au NPs on the  $\text{Fe}_3\text{O}_4$  NPs surfaces increased. This is attributed to a greater amount of  $\text{NH}_2$  groups provided by PEI that can adsorb more Au NPs with an increase in the PEI concentration.

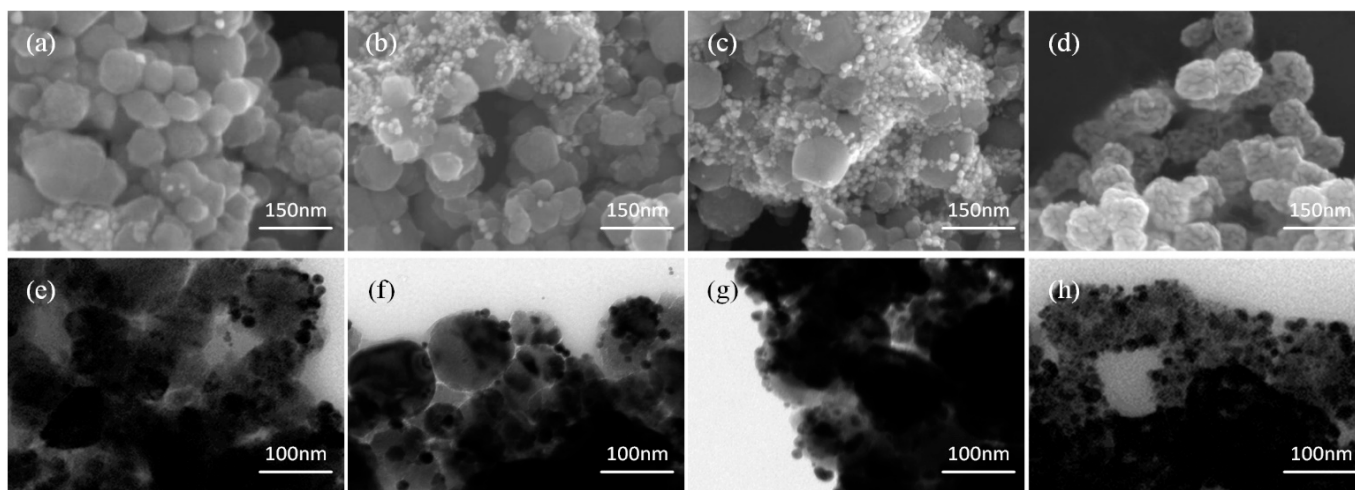


**Figure 4.** SEM images of the  $\text{Fe}_3\text{O}_4$ -PEI-Au NPs treated with (a) 5, (b) 15, (c) 25, and (d) 35 mg/mL PEI solution. The corresponding TEM images of the  $\text{Fe}_3\text{O}_4$ -PEI-Au NPs treated with (e) 5, (f) 15, (g) 25, and (h) 35 mg/mL PEI solution.

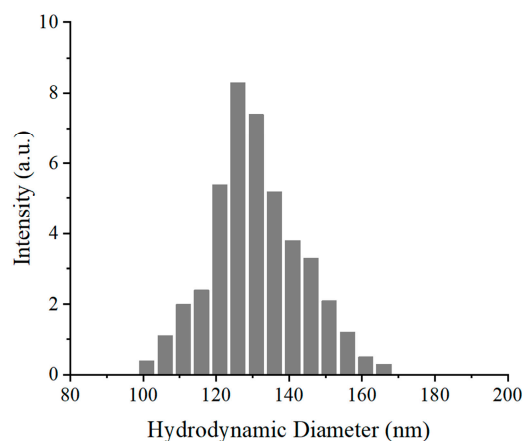


**Figure 5.** Hydrodynamic diameter distribution of  $\text{Fe}_3\text{O}_4$ -PEI-Au NPs (PEI: 35 mg/mL).

### 3.2.2. X-ray Diffraction (XRD) Analysis

An X-ray diffractometer was used to characterize the crystal structures of the  $\text{Fe}_3\text{O}_4$  and  $\text{Fe}_3\text{O}_4$ -PEI-Au NPs. As shown in Figure 6a, the XRD spectrum of  $\text{Fe}_3\text{O}_4$  showed six diffraction peaks at  $2\theta$  values of  $30.43^\circ$ ,  $35.78^\circ$ ,  $43.44^\circ$ ,  $53.79^\circ$ ,  $57.34^\circ$ , and  $62.89^\circ$ , corresponding to the diffraction peaks located at (220), (311), (400), (422), (511), and (440). All these diffraction peaks correspond to the face-centered cubic structure of  $\text{Fe}_3\text{O}_4$ . Compared to that of  $\text{Fe}_3\text{O}_4$ , the XRD spectrum of the  $\text{Fe}_3\text{O}_4$ -PEI-Au NPs exhibited additional peaks at  $38.62^\circ$ ,  $44.67^\circ$ ,  $64.61^\circ$ , and  $77.62^\circ$ , which match well with the (111), (200), (220), and (311) faces of Au. This result is consistent with that reported in the literature [54]. Therefore, the

X-ray diffraction spectra further confirmed that Au NPs were successfully loaded onto the  $\text{Fe}_3\text{O}_4$  NPs surfaces. In addition, in Figure 6b, it is implied that with an increase in the PEI concentration, the characteristic peak intensities of the Au NPs gradually increased, while the characteristic peak intensities of the  $\text{Fe}_3\text{O}_4$  NPs gradually decreased. This is because of the increase in the density of Au NPs coated on the  $\text{Fe}_3\text{O}_4$  NPs surfaces. No peaks of other impurities were detected in the XRD spectra, indicating a high purity of the materials.

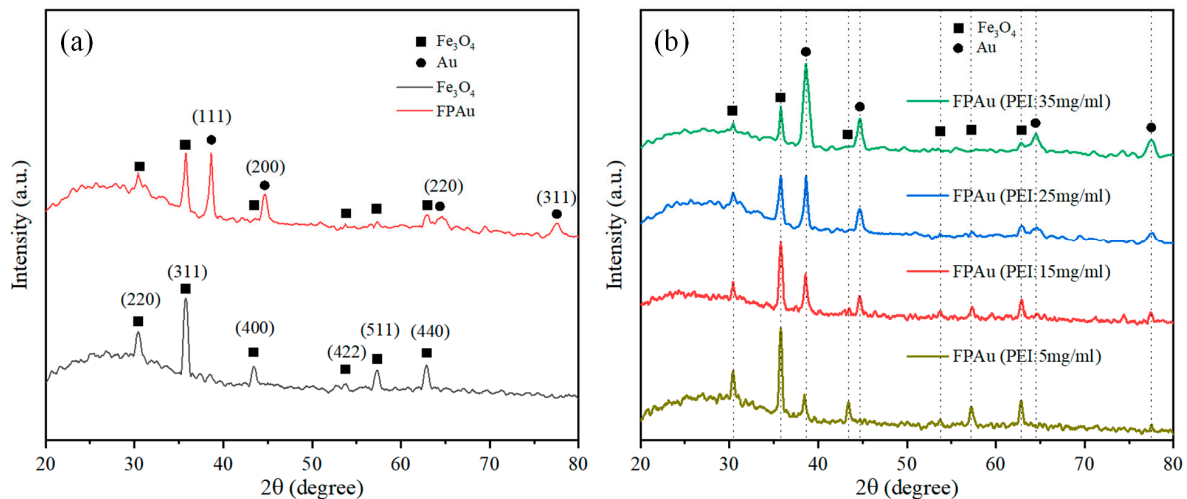


**Figure 6.** XRD spectra of the (a)  $\text{Fe}_3\text{O}_4$  and  $\text{Fe}_3\text{O}_4$ -PEI-Au (FPAu) NPs, and (b)  $\text{Fe}_3\text{O}_4$ -PEI-Au (FPAu) NPs treated with 5–35 mg/mL PEI solution.

### 3.2.3. Analysis of Magnetic and Plasmonic Properties

Firstly, the magnetic properties of the  $\text{Fe}_3\text{O}_4$ -PEI-Au NPs with different coverages of the Au NPs on the  $\text{Fe}_3\text{O}_4$  NPs surfaces were studied. Figure 7a exhibits the hysteresis loops of the  $\text{Fe}_3\text{O}_4$ -PEI-Au NPs with different Au NP densities, controlled by using different PEI concentrations (the magnetic field scanning range was 20,000 g at 300 K). All the curves for the  $\text{Fe}_3\text{O}_4$  and  $\text{Fe}_3\text{O}_4$ -PEI-Au NPs have similar shapes. The saturation magnetization of the  $\text{Fe}_3\text{O}_4$  NPs was 60 emu/g, which is same as that of  $\text{Fe}_3\text{O}_4$  NPs in a previous study [55]. After treatment with the PEI solution, the saturation magnetization of the  $\text{Fe}_3\text{O}_4$ -PEI NPs decreased to 57 emu/g. This value is a little smaller than the one previously reported for PEI-coated  $\text{Fe}_3\text{O}_4$  NPs [56]. This may be due to the agglomeration of particles and the interaction between them [55]. Furthermore, for the  $\text{Fe}_3\text{O}_4$ -PEI-Au NPs, when the PEI concentration increased from 5 to 35 mg/mL, the Au NP coating density increased, and the saturation magnetization of the  $\text{Fe}_3\text{O}_4$ -PEI-Au NPs decreased from 55 to 16 emu/g, as shown in Table 1. The reduction in saturation magnetization of the  $\text{Fe}_3\text{O}_4$  NPs due to the introduction of plasmonic metal NPs could be demonstrated in reference [54]. Therefore, with the increase in the density of the Au NPs on the  $\text{Fe}_3\text{O}_4$  NPs surfaces, the shielding effect of the Au NPs on the  $\text{Fe}_3\text{O}_4$  NPs increases.

**Table 1.** Absorption peak wavelength and saturation magnetization of the  $\text{Fe}_3\text{O}_4$ , Au,  $\text{Fe}_3\text{O}_4$ -PEI-Au nanoparticles treated with different PEI concentrations.

	$\text{Fe}_3\text{O}_4$	Au	$\text{Fe}_3\text{O}_4$ -PEI-Au PEI: 5 mg/mL	$\text{Fe}_3\text{O}_4$ -PEI-Au PEI: 15 mg/mL	$\text{Fe}_3\text{O}_4$ -PEI-Au PEI: 25 mg/mL	$\text{Fe}_3\text{O}_4$ -PEI-Au PEI: 35 mg/mL
Absorption peak (nm)	/	519	526	535	552	578
Saturation magnetization (emu/g)	60	/	55	46	31	16

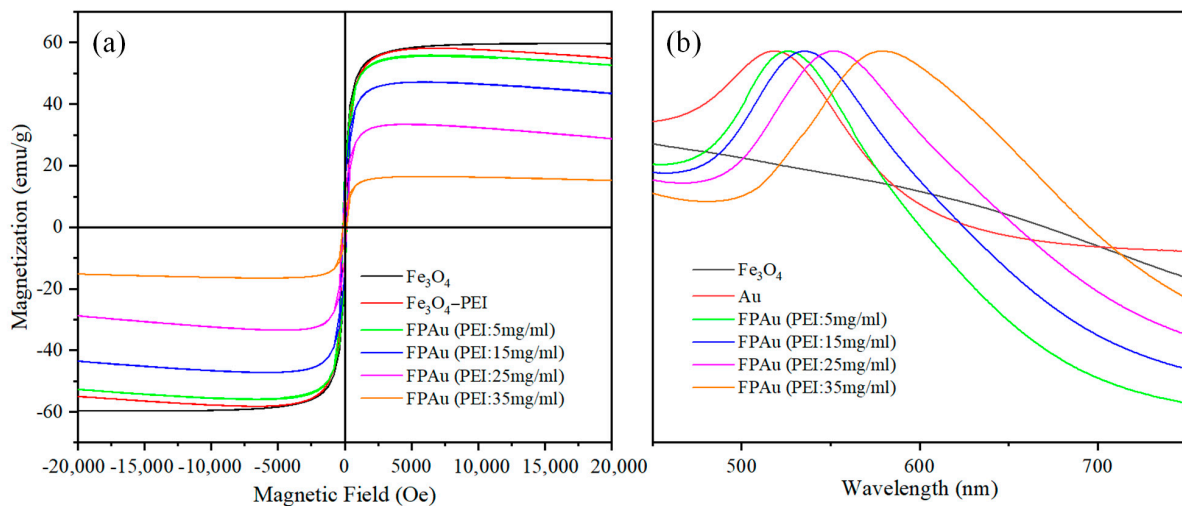


**Figure 7.** (a) Hysteresis loops and (b) normalized absorption spectra of the Fe<sub>3</sub>O<sub>4</sub> and Fe<sub>3</sub>O<sub>4</sub>-PEI-Au (FPAu) NPs treated with 5~35 mg/mL PEI solution.

Due to Fe<sub>3</sub>O<sub>4</sub>-PEI-Au NPs with different Au NP densities exhibiting different magnetic and plasmonic properties, we also investigated the plasmonic properties of the Fe<sub>3</sub>O<sub>4</sub>-PEI-Au NPs. Figure 7b shows the absorption spectra of the Fe<sub>3</sub>O<sub>4</sub>-PEI-Au NPs with different Au NP densities. The Fe<sub>3</sub>O<sub>4</sub> NPs had no absorption peak in the visible region, which is consistent with the result from a previous study [57]. The absorption peak of the Au NPs was located at 519 nm. When the PEI concentration increased from 5 to 35 mg/mL, the Au NP coating density increased and the absorption peak of the Fe<sub>3</sub>O<sub>4</sub>-PEI-Au NPs red shifted from 526 to 578 nm (shown in Table 1) because of the decrease in the gap distance between the Au NPs. To further investigate the influence of the Au NP coating density on the enhanced electric field of the nanoparticles, three-dimensional models of the Fe<sub>3</sub>O<sub>4</sub> nanoparticle decorated with different Au NP densities were built. Many researchers calculated electric field characteristics by quantum method [58], or classical method [59,60]. Here, the electric field distributions were simulated using the finite element method with the commercial software COMSOL 5.5. Figure 8 shows the electric field distributions of Au-decorated Fe<sub>3</sub>O<sub>4</sub> NPs with Au NP coating densities ranging from sparse to dense. It was observed that with an increase in the Au NP coating density, the electric field became stronger, and the plasmonic coupling between the adjacent nanoparticles became stronger, indicating that the plasmonic properties were enhanced.

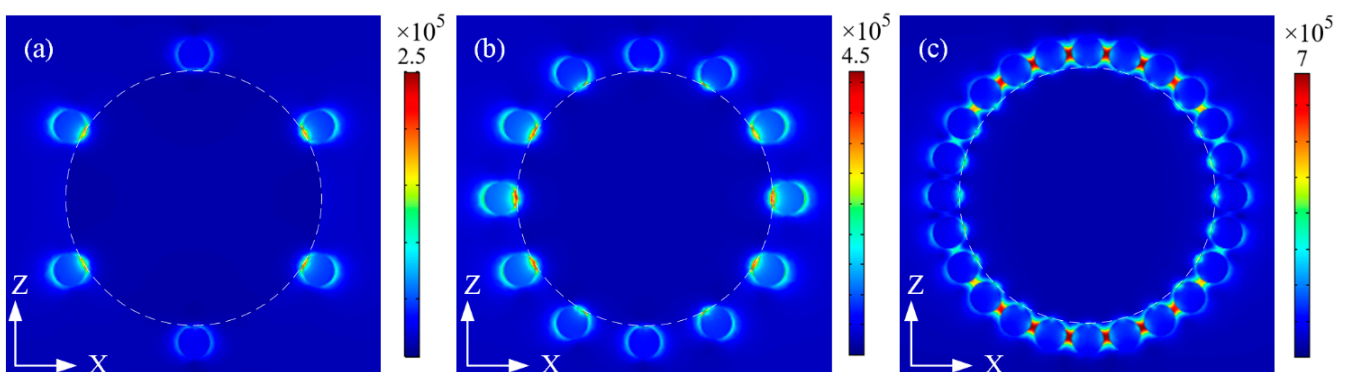


**Figure 8.** Electric field distributions of the Fe<sub>3</sub>O<sub>4</sub> NP coating with Au NPs of (a) sparse, (b) medium, and (c) dense.

### 3.3. Study on the Properties of the $\text{Fe}_3\text{O}_4$ -PEI-Ag Nanoparticles

#### 3.3.1. $\text{Fe}_3\text{O}_4$ -PEI-Ag Nanoparticles

According to Figure 7b, the plasmonic resonance peak of the  $\text{Fe}_3\text{O}_4$ -PEI-Au NPs is located at about 526 nm. However, when a shorter wavelength of plasmonic resonance is needed,  $\text{Fe}_3\text{O}_4$ -PEI-Ag NPs are more suitable; thus, we also need to study their magnetic and plasmonic properties. Here, we synthesized  $\text{Fe}_3\text{O}_4$ -PEI-Ag NPs using the same methods that were utilized to prepare the  $\text{Fe}_3\text{O}_4$ -PEI-Au NPs. Similarly, positively charged PEI binds to negatively charged  $\text{Fe}_3\text{O}_4$  by electrostatic self-assembly, and negatively charged Ag nanoparticles combine with positively charged PEI-coated  $\text{Fe}_3\text{O}_4$  nanoparticles to form  $\text{Fe}_3\text{O}_4$ -PEI-Ag NPs. Figure 9 shows SEM and TEM images of the Ag-decorated  $\text{Fe}_3\text{O}_4$  NPs treated with PEI concentrations ranging from 5 to 35 mg/mL. It was observed that 10 nm diameter Ag NPs were attached to the surface of 80 nm diameter  $\text{Fe}_3\text{O}_4$  NPs. DLS measurements show that the hydrodynamic diameter of the  $\text{Fe}_3\text{O}_4$ -PEI-Ag NPs is about 137 nm (as shown in Figure 10) and the zeta potential is around +19.1 mV. When the  $\text{Fe}_3\text{O}_4$  NPs were treated with a 5 mg/mL PEI solution, a small amount of Ag NP was coated on the  $\text{Fe}_3\text{O}_4$  NP surfaces, as shown in Figure 9a,e. When the concentration of PEI increased from 5 to 35 mg/mL, the coverage of the Ag NPs on the  $\text{Fe}_3\text{O}_4$  NPs surfaces increased gradually. This is because of the greater amount of  $\text{NH}_2$  groups provided by the PEI leading to an increased number of Ag NPs attached on the  $\text{Fe}_3\text{O}_4$  surface with the increase in PEI concentration.

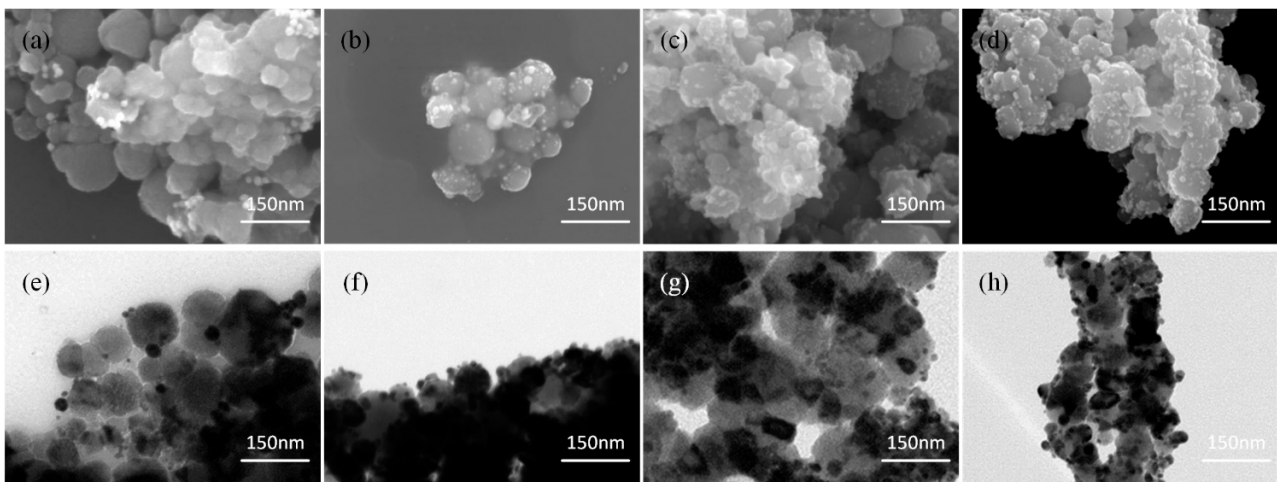


**Figure 9.** SEM images of the  $\text{Fe}_3\text{O}_4$ -PEI-Ag NPs treated with (a) 5, (b) 15, (c) 25, and (d) 35 mg/mL PEI solution. The corresponding TEM images of the  $\text{Fe}_3\text{O}_4$ -PEI-Ag NPs treated with (e) 5, (f) 15, (g) 25, and (h) 35 mg/mL PEI solution.

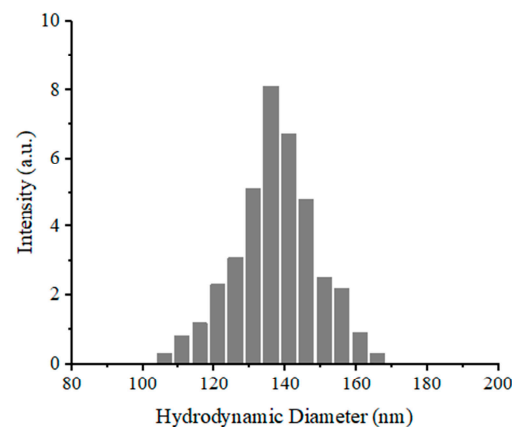


**Figure 10.** Hydrodynamic diameter distribution of  $\text{Fe}_3\text{O}_4$ -PEI-Ag NPs (PEI: 35 mg/mL).

### 3.3.2. X-ray Diffraction Analysis

The crystalline structures of the  $\text{Fe}_3\text{O}_4$  and  $\text{Fe}_3\text{O}_4$ -PEI-Ag NPs were characterized using an X-ray diffractometer. As shown in Figure 11a, the positions and relative intensities of all diffraction peaks are in good agreement with the standard  $\text{Fe}_3\text{O}_4$  and Ag NP diffraction peaks. Compared to the  $\text{Fe}_3\text{O}_4$  NPs, there were four more main peaks in the  $\text{Fe}_3\text{O}_4$ -PEI-Ag NP spectrum, which can be clearly observed at  $2\theta$  values of  $38.42^\circ$ ,  $44.63^\circ$ ,  $64.53^\circ$ , and  $77.38^\circ$ , corresponding to the reflection of the (111), (200), (220), and (311) crystal planes of Ag [61]. Therefore, the X-ray diffraction spectra further confirmed that Ag NPs were successfully loaded on the  $\text{Fe}_3\text{O}_4$  NPs surfaces. In addition, Figure 11b shows that, with an increase in the PEI concentration, the characteristic peak intensities of the Ag NPs gradually increased, while that of the  $\text{Fe}_3\text{O}_4$  NPs gradually decreased. This is because of the increase in the density of Ag NPs coated on the  $\text{Fe}_3\text{O}_4$  NPs surfaces. No peaks of other impurities were detected in the XRD spectra, indicating high purity of the materials.

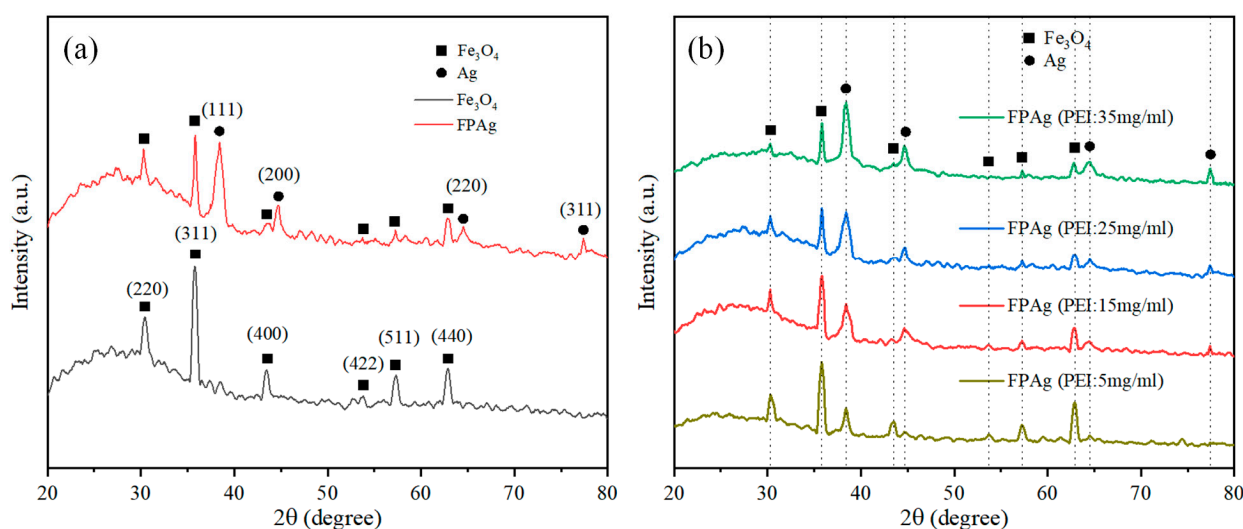


**Figure 11.** XRD spectra of the (a)  $\text{Fe}_3\text{O}_4$  and  $\text{Fe}_3\text{O}_4$ -PEI-Ag (FPAg) NPs, and (b)  $\text{Fe}_3\text{O}_4$ -PEI-Ag (FPAg) NPs treated with 5–35 mg/mL PEI solution.

### 3.3.3. Analysis of Magnetic and Plasmonic Properties

Figure 12a illustrates the hysteresis loops of the Ag-decorated  $\text{Fe}_3\text{O}_4$  NPs treated with different PEI concentrations. It can be observed that the curves of the  $\text{Fe}_3\text{O}_4$  and  $\text{Fe}_3\text{O}_4$ -PEI-Ag NPs exhibit similar trends. The saturation magnetization of the  $\text{Fe}_3\text{O}_4$  NPs was 60 emu/g. When the PEI concentration increased from 5 to 35 mg/mL, the Ag NP coating density increased, and the saturation magnetization of the  $\text{Fe}_3\text{O}_4$ -PEI-Ag NPs decreased from 56 to 22 emu/g, as shown in Table 2. Therefore, with an increase in the Ag NP density, the shielding effect of the Ag NPs coated on the  $\text{Fe}_3\text{O}_4$  NPs increases.

**Table 2.** Absorption peak and saturation magnetization of  $\text{Fe}_3\text{O}_4$ , Ag, and  $\text{Fe}_3\text{O}_4$ -PEI-Ag nanoparticles treated with different PEI concentrations.

	$\text{Fe}_3\text{O}_4$	Ag	$\text{Fe}_3\text{O}_4$ -PEI-Ag PEI: 5 mg/mL	$\text{Fe}_3\text{O}_4$ -PEI-Ag PEI: 15 mg/mL	$\text{Fe}_3\text{O}_4$ -PEI-Ag PEI: 25 mg/mL	$\text{Fe}_3\text{O}_4$ -PEI-Ag PEI: 35 mg/mL
Absorption peak (nm)	/	406	417	425	442	472
Saturation magnetization (emu/g)	60	/	56	49	36	22

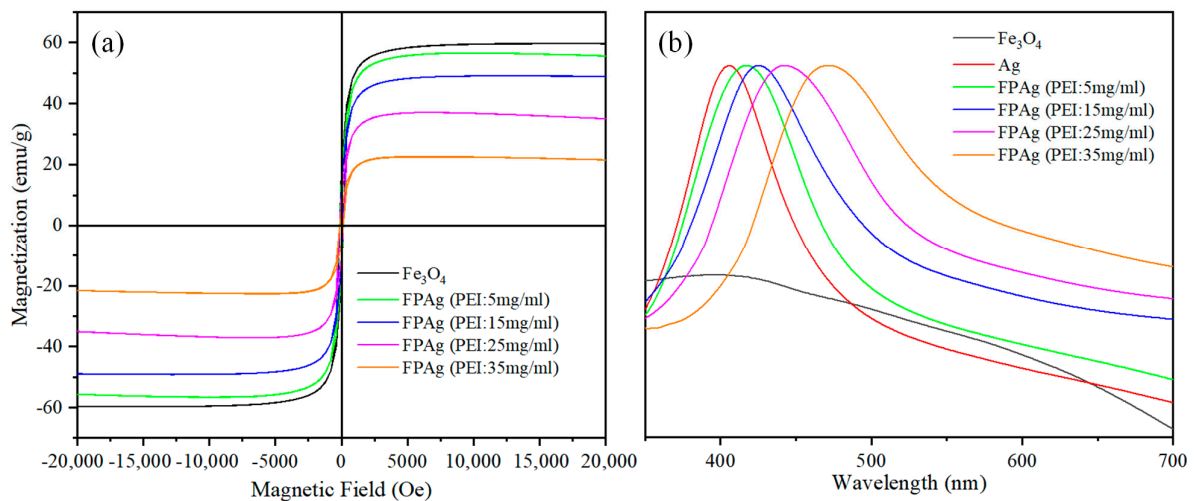


**Figure 12.** (a) Hysteresis loops and (b) normalized absorption spectra of the Fe<sub>3</sub>O<sub>4</sub> and Fe<sub>3</sub>O<sub>4</sub>–PEI–Ag (FPAg) NPs treated with 5–35 mg/mL PEI solution.

Figure 12b shows the absorption spectra of the Ag and Fe<sub>3</sub>O<sub>4</sub>–PEI–Ag NPs. It shows that 10 nm Ag NPs had a plasmonic absorption peak of 406 nm. When the PEI concentration increased from 5 to 35 mg/mL, the absorption peak of the Fe<sub>3</sub>O<sub>4</sub>–PEI–Ag NPs red shifted from 417 to 472 nm with the increase in the Ag NP coating density (Table 2). This is due to the decrease in the gap distance between the Ag NPs. To further study the effect of Ag NP coating density on the enhanced electric field of the nanoparticles, the electric field distributions were simulated using the finite element method. Figure 13 illustrates the electric field distributions of Ag-decorated Fe<sub>3</sub>O<sub>4</sub> NPs with varying Ag NP coating densities ranging from sparse to dense. It was found that, as the coating density increased, the electric field became stronger. Therefore, according to the analysis of the magnetic and plasmonic properties of Au- or Ag-decorated Fe<sub>3</sub>O<sub>4</sub> NPs treated with different PEI concentrations, as shown in Figure 7, Figure 8, Figure 12, and Figure 13, it is implied that when the PEI concentration is low, such as 5 mg/mL, the coverage of plasmonic metal NPs on the surface of Fe<sub>3</sub>O<sub>4</sub> NPs is minimal. This results in a weak shielding effect of plasmonic metal NPs, leading to a strong magnetic field intensity but a weak plasmonic intensity in Fe<sub>3</sub>O<sub>4</sub>–PEI–M (M = Au or Ag) NPs. Conversely, when the PEI concentration is high (such as 35 mg/mL), the coverage of the plasmonic metal NPs is too large, the shielding effect of the plasmonic metal NPs is strong, the magnetic intensity becomes weak, and the plasmonic intensity becomes strong. Therefore, when the PEI concentration is between 15 and 25 mg/mL, there is an optimal coverage of the plasmonic metal NPs on the Fe<sub>3</sub>O<sub>4</sub> NP surfaces to balance the magnetic and plasmonic properties.

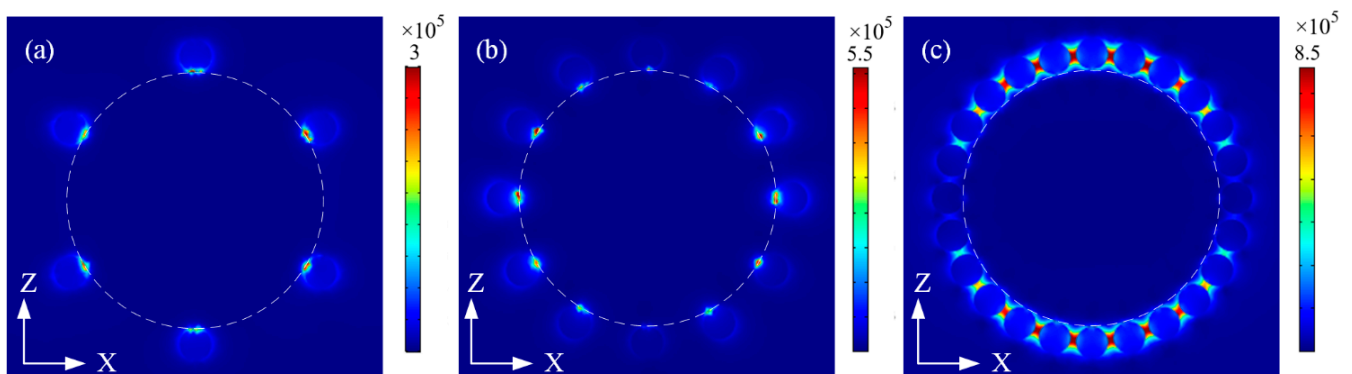


**Figure 13.** Electric field distributions of the Fe<sub>3</sub>O<sub>4</sub> NP coating with Ag NPs of (a) sparse, (b) medium, (c) dense.

#### 4. Conclusions

In conclusion, we synthesized Fe<sub>3</sub>O<sub>4</sub>-PEI-M (M = Au or Ag) NPs using a simple method. The density of the plasmonic metal NPs coated on the Fe<sub>3</sub>O<sub>4</sub> NPs surfaces was adjusted by controlling the PEI concentration. We investigated the effects of the Au or Ag NP coating density on the magnetic and plasmonic properties of the Fe<sub>3</sub>O<sub>4</sub>-PEI-M (M = Au or Ag) NPs. We found that, for the Fe<sub>3</sub>O<sub>4</sub>-PEI-M (M = Au or Ag) NPs, with an increase in the plasmonic metal NP density, the saturation magnetization decreased, the plasmonic intensity increased, and the plasmonic absorption peak was red shifted. When the concentration of PEI was between 15 and 25 mg/mL, Fe<sub>3</sub>O<sub>4</sub>-PEI-M (M = Au or Ag) NPs exhibited both excellent magnetic and plasmonic properties. The relationships among the coating density of the plasmonic metal NPs and both magnetic and plasmonic properties were established. This work can provide guidance for the application of Fe<sub>3</sub>O<sub>4</sub>-M (M = Au or Ag) NPs in the biomedical field.

**Author Contributions:** Conceptualization, S.N.; methodology, S.W.; investigation, Z.L., B.Y. and F.Z.; resources, N.Z.; data curation, S.W.; writing—original draft preparation, S.W.; writing—review and editing, S.N.; funding acquisition, N.Z. All authors have read and agreed to the published version of the manuscript.

**Funding:** This work was supported by the National Natural Science Foundation of China under Grant (62375163 and 52177225), the Key Research and Development Program of Shaanxi Province (2023-YBSF-126), the China Postdoctoral Science Foundation under Grant (2019M653635).

**Institutional Review Board Statement:** Not applicable.

**Informed Consent Statement:** Not applicable.

**Data Availability Statement:** Data are contained within the article.

**Conflicts of Interest:** The authors declare no conflicts of interest.

#### References

1. Price, P.M.; Mahmoud, W.E.; Al-Ghamdi, A.A.; Bronstein, L.M. Magnetic Drug Delivery: Where the Field Is Going. *Front. Chem.* **2018**, *6*, 619. [[CrossRef](#)] [[PubMed](#)]
2. Fang, Z.; Li, X.; Xu, Z.; Du, F.; Wang, W.; Shi, R.; Gao, D. Hyaluronic acid-modified mesoporous silica-coated superparamagnetic Fe<sub>3</sub>O<sub>4</sub> nanoparticles for targeted drug delivery. *Int. J. Nanomed.* **2019**, *14*, 5785–5797. [[CrossRef](#)] [[PubMed](#)]
3. Mokhodoeva, O.; Vlč, M.; Málková, E.; Kukleva, E.; Mičolová, P.; Štamberg, K.; Šlouf, M.; Dzheloda, R.; Kozempel, J. Study of <sup>223</sup>Ra uptake mechanism by Fe<sub>3</sub>O<sub>4</sub> nanoparticles: Towards new prospective theranostic SPIONs. *J. Nanoparticle Res.* **2016**, *18*, 301. [[CrossRef](#)]
4. Efimova, N.V.; Krasnopyorova, A.P.; Yuhno, G.D.; Sofronov, D.S.; Rucki, M. Uptake of Radionuclides <sup>60</sup>Co, <sup>137</sup>Cs, and <sup>90</sup>Sr with α-Fe<sub>2</sub>O<sub>3</sub> and Fe<sub>3</sub>O<sub>4</sub> Particles from Aqueous Environment. *Materials* **2021**, *14*, 2899. [[CrossRef](#)] [[PubMed](#)]
5. Lu, Q.; Dai, X.; Zhang, P.; Tan, X.; Zhong, Y.; Yao, C.; Song, M.; Song, G.; Zhang, Z.; Peng, G.; et al. Fe<sub>3</sub>O<sub>4</sub>@Au composite magnetic nanoparticles modified with cetuximab for targeted magneto-photothermal therapy of glioma cells. *Int. J. Nanomed.* **2018**, *13*, 2491–2505. [[CrossRef](#)] [[PubMed](#)]
6. Fotukian, S.M.; Barati, A.; Soleymani, M.; Alizadeh, A.M. Solvothermal synthesis of CuFe<sub>2</sub>O<sub>4</sub> and Fe<sub>3</sub>O<sub>4</sub> nanoparticles with high heating efficiency for magnetic hyperthermia application. *J. Alloys Compd.* **2020**, *816*, 152548. [[CrossRef](#)]
7. Qu, J.; Liu, G.; Wang, Y.; Hong, R. Preparation of Fe<sub>3</sub>O<sub>4</sub>-chitosan nanoparticles used for hyperthermia. *Adv. Powder Technol.* **2010**, *21*, 461–467. [[CrossRef](#)]
8. Żuk, M.; Podgórski, R.; Ruszczyńska, A.; Ciach, T.; Majkowska-Pilip, A.; Bilewicz, A.; Krysiński, P. Multifunctional Nanoparticles Based on Iron Oxide and Gold-198 Designed for Magnetic Hyperthermia and Radionuclide Therapy as a Potential Tool for Combined HER2-Positive Cancer Treatment. *Pharmaceutics* **2022**, *14*, 1680. [[CrossRef](#)]
9. Dukenbayev, K.; Korolkov, I.V.; Tishkevich, D.I.; Kozlovskiy, A.L.; Trukhanov, S.V.; Gorin, Y.G.; Shumskaya, E.E.; Kaniukov, E.Y.; Vinnik, D.A.; Zdorovets, M.V.; et al. Fe<sub>3</sub>O<sub>4</sub> Nanoparticles for Complex Targeted Delivery and Boron Neutron Capture Therapy. *Nanomaterials* **2019**, *9*, 494. [[CrossRef](#)]
10. Shen, L.; Li, B.; Qiao, Y. Fe<sub>3</sub>O<sub>4</sub> Nanoparticles in Targeted Drug/Gene Delivery Systems. *Materials* **2018**, *11*, 324. [[CrossRef](#)]
11. Luan, D.; Zheng, A.; Gao, X.; Xu, K.; Tang, B. Fishing out Methionine-Containing Proteins from Complex Biological Systems Based on a Non-Enzymatic Biochemical Reaction. *Nano Lett.* **2021**, *21*, 209–215. [[CrossRef](#)] [[PubMed](#)]
12. Kristianto, H.; Reynaldi, E.; Prasetyo, S.K.; Sugih, A. Adsorbed leucaena protein on citrate modified Fe<sub>3</sub>O<sub>4</sub> nanoparticles: Synthesis, characterization, and its application as magnetic coagulant. *Environ. Res.* **2020**, *30*, 32. [[CrossRef](#)]

13. Jose, L.; Lee, C.; Hwang, A.; Park, J.H.; Song, J.K.; Paik, H. Magnetically steerable Fe<sub>3</sub>O<sub>4</sub>@Ni<sup>2+</sup>-NTA-polystyrene nanoparticles for the immobilization and separation of his6-protein. *Eur. Polym. J.* **2019**, *112*, 524–529. [[CrossRef](#)]
14. Loh, K.S.; Lee, Y.H.; Musa, A.; Salmah, A.A.; Zamri, I. Use of Fe<sub>3</sub>O<sub>4</sub> Nanoparticles for Enhancement of Biosensor Response to the Herbicide 2,4-Dichlorophenoxyacetic Acid. *Sensors* **2008**, *8*, 5775–5791. [[CrossRef](#)] [[PubMed](#)]
15. Zhang, Z.; Wang, X.; Yang, X. A sensitive choline biosensor using Fe<sub>3</sub>O<sub>4</sub> magnetic nanoparticles as peroxidase mimics. *Analyst* **2011**, *136*, 4960–4965. [[CrossRef](#)] [[PubMed](#)]
16. Kore, R.; Sawant, A.D.; Rogers, R.D. Recyclable Magnetic Fe<sub>3</sub>O<sub>4</sub> Nanoparticle-Supported Chloroaluminate Ionic Liquids for Heterogeneous Lewis Acid Catalysis. *ACS Sustain. Chem. Eng.* **2021**, *9*, 8797–8802. [[CrossRef](#)]
17. Li, S.; Zhao, X.; Yu, X.; Wan, Y.; Yin, M.; Zhang, W.; Cao, B.; Wang, H. Fe<sub>3</sub>O<sub>4</sub> Nanozymes with Aptamer-Tuned Catalysis for Selective Colorimetric Analysis of ATP in Blood. *Anal. Chem.* **2019**, *91*, 14737–14742. [[CrossRef](#)]
18. Akram, N.; Ma, W.; Guo, J.; Guo, Y.; Zhao, Y.; Hassan, A.; Wang, J. Synergistic catalysis of Fe<sub>3</sub>O<sub>4</sub>/CuO bimetallic catalyst derived from Prussian blue analogues for the efficient decomposition of various organic pollutants. *Chem. Phys.* **2021**, *540*, 110974. [[CrossRef](#)]
19. Sohn, C.H.; Park, S.P.; Choi, S.H.; Park, S.H.; Kim, S.; Xu, L.; Kim, S.H.; Hur, J.A.; Choi, J.; Choi, T.H. MRI molecular imaging using GLUT1 antibody-Fe<sub>3</sub>O<sub>4</sub> nanoparticles in the hemangioma animal model for differentiating infantile hemangioma from vascular malformation. *Nanomedicine* **2015**, *11*, 127–135. [[CrossRef](#)]
20. Zou, X.; Li, K.; Zhao, Y.; Zhang, Y.; Li, B.; Song, C. Ferroferric oxide/l-cysteine magnetic nanospheres for capturing histidine-tagged proteins. *J. Mater. Chem. B* **2013**, *1*, 5108–5113. [[CrossRef](#)]
21. Gawali, S.L.; Shelar, S.B.; Gupta, J.; Barick, K.C.; Hassan, P.A. Immobilization of protein on Fe<sub>3</sub>O<sub>4</sub> nanoparticles for magnetic hyperthermia application. *Int. J. Biol. Macromol.* **2021**, *166*, 851–860. [[CrossRef](#)] [[PubMed](#)]
22. Li, C.H.; Chan, M.H.; Chang, Y.C.; Hsiao, M. Gold Nanoparticles as a Biosensor for Cancer Biomarker Determination. *Molecules* **2023**, *28*, 364. [[CrossRef](#)] [[PubMed](#)]
23. Xu, Z.; Hou, Y.; Sun, S. Magnetic core/shell Fe<sub>3</sub>O<sub>4</sub>/Au and Fe<sub>3</sub>O<sub>4</sub>/Au/Ag nanoparticles with tunable plasmonic properties. *J. Am. Chem. Soc.* **2007**, *129*, 8698–8699. [[CrossRef](#)] [[PubMed](#)]
24. Ramesh, R.; Geerthana, M.; Prabhu, S.; Sohila, S. Synthesis and Characterization of the Superparamagnetic Fe<sub>3</sub>O<sub>4</sub>/Ag Nanocomposites. *J. Clust. Sci.* **2017**, *28*, 963–969. [[CrossRef](#)]
25. Abdollahi, S.N.; Naderi, M.; Amoabediny, G. Synthesis and physicochemical characterization of tunable silica-gold nanoshells via seed growth method. *Colloids Surf. A Physicochem. Eng. Asp.* **2012**, *414*, 345–351. [[CrossRef](#)]
26. Abkenar, A.K.; Naderi, M. Chemical synthesis of gold nanoparticles with different morphology from a secondary source. *J. Iran. Chem. Soc.* **2016**, *13*, 2173–2184. [[CrossRef](#)]
27. Rajan, A.; Vilas, V.; Philip, D. Studies on catalytic, antioxidant, antibacterial and anticancer activities of biogenic gold nanoparticles. *J. Mol. Liq.* **2015**, *212*, 331–339. [[CrossRef](#)]
28. Lie, J.; Huang, J.; You, R.; Lu, Y. Preparation and Application of Magnetic Molecularly Imprinted Plasmonic SERS Composite Nanoparticles. *Crit. Rev. Anal. Chem.* **2023**, 1–20. [[CrossRef](#)]
29. Han, D.; Li, B.; Chen, Y.; Wu, T.; Kou, Y.; Xue, X.; Chen, L.; Liu, Y.; Duan, Q. Facile synthesis of Fe<sub>3</sub>O<sub>4</sub>@Au core-shell nanocomposite as a recyclable magnetic surface enhanced Raman scattering substrate for thiram detection. *Nanotechnology* **2019**, *30*, 465703. [[CrossRef](#)]
30. Dheyab, A.M.; Aziz, A.A.; Jameel, M.S.; Khaniabadi, M.P. Recent Advances in Synthesis, Medical Applications and Challenges for Gold-Coated Iron Oxide: Comprehensive Study. *Nanomaterials* **2021**, *11*, 2147. [[CrossRef](#)]
31. Liu, C.H.; Zhou, Z.D.; Yu, X.; Lv, B.Q.; Mao, J.F.; Xiao, D. Preparation and characterization of Fe<sub>3</sub>O<sub>4</sub>/Ag composite magnetic nanoparticles. *Inorg. Mater.* **2008**, *44*, 291–295. [[CrossRef](#)]
32. Rajkumar, S.; Prabakaran, M. Theranostics Based on Iron Oxide and Gold Nanoparticles for Imaging-Guided Photothermal and Photodynamic Therapy of Cancer. *Curr. Top. Med. Chem.* **2017**, *17*, 1858–1871. [[CrossRef](#)] [[PubMed](#)]
33. Jiang, W.; Zhou, Y.; Zhang, Y.; Xuan, S.; Gong, X. Superparamagnetic Ag@Fe<sub>3</sub>O<sub>4</sub> core-shell nanospheres: Fabrication, characterization and application as reusable nanocatalysts. *Dalton Trans.* **2012**, *41*, 4594–4601. [[CrossRef](#)] [[PubMed](#)]
34. Gai, K.; Qi, H.; Li, X.; Liu, X. Detection of Residual Methomyl in Vegetables with an Electrochemical Sensor based on a glassy carbon electrode modified with Fe<sub>3</sub>O<sub>4</sub>/Ag composite. *Int. J. Electrochem. Sci.* **2019**, *14*, 1283–1292. [[CrossRef](#)]
35. Amarjargal, A.; Tijing, L.D.; Im, I.T.; Kim, C.S. Simultaneous preparation of Ag/Fe<sub>3</sub>O<sub>4</sub> core-shell nanocomposites with enhanced magnetic moment and strong antibacterial and catalytic properties. *Chem. Eng. J.* **2013**, *226*, 243–254. [[CrossRef](#)]
36. Benvidi, A.; Jahanbani, S. Self-assembled monolayer of SH-DNA strand on a magnetic bar carbon paste electrode modified with Fe<sub>3</sub>O<sub>4</sub>@Ag nanoparticles for detection of breast cancer mutation. *J. Electroanal. Chem.* **2016**, *768*, 47–54. [[CrossRef](#)]
37. Kou, Y.; Wu, T.; Xing, G.; Huang, X.; Han, D.; Yang, S.; Guo, C.; Gao, W.; Yang, J.; Liu, Y.; et al. Highly efficient and recyclable catalyst: Porous Fe<sub>3</sub>O<sub>4</sub>-Au magnetic nanocomposites with tailored synthesis. *Nanotechnology* **2020**, *31*, 225701. [[CrossRef](#)]
38. Aarthi, A.; Umadevi, M.; Parimaladevi, R.; Sathe, G.V.; Arumugam, S.; Sivaprakash, P. A Negatively Charged Hydrophobic Hemi-micelle of Fe<sub>3</sub>O<sub>4</sub>/Ag MNP Role Towards SERS, Photocatalysis and Bactericidal. *J. Inorg. Organomet. Polym. Mater.* **2021**, *31*, 1469–1479. [[CrossRef](#)]
39. Oguzlar, S. Development of highly sensitive [Ru(bpy)<sub>3</sub>]<sup>2+</sup>-Based optical oxygen sensing thin films in the presence with Fe<sub>3</sub>O<sub>4</sub> and Fe<sub>3</sub>O<sub>4</sub>@Ag NPs. *Opt. Mater.* **2020**, *101*, 109772. [[CrossRef](#)]

40. Du, B.W.; Chu, C.Y.; Lin, C.C.; Ko, F.H. The Multifunctionally Graded System for a Controlled Size Effect on Iron Oxide–Gold Based Core-Shell Nanoparticles. *Nanomaterials* **2021**, *11*, 1695. [[CrossRef](#)]
41. Salimi, Z.; Ehsani, M.H.; Dezfuli, A.S.; Alamzadeh, Z. Evaluation of Iron and Au-Fe<sub>3</sub>O<sub>4</sub> Ferrite Nanoparticles for Biomedical Application. *J. Supercond. Nov. Magn.* **2022**, *35*, 215–222. [[CrossRef](#)]
42. Lv, X.; Fang, Z.; Sun, Y.; Yang, Y.; Wang, X.; Chen, Y.; Qin, Y.; Li, N.; Li, C.; Xu, J.; et al. Interfacial preparation of multi-branched magneto-plasmonic Fe<sub>3</sub>O<sub>4</sub>@Au core@shell nanocomposites as efficient photothermal agents for antibacterial application. *J. Alloys Compd.* **2023**, *932*, 167712. [[CrossRef](#)]
43. Mikoliunaite, L.; Talaikis, M.; Michalowska, A.; Dobilas, J.; Stankevic, V.; Kudelski, A.; Niaura, G. Thermally Stable Magneto-Plasmonic Nanoparticles for SERS with Tunable Plasmon Resonance. *Nanomaterials* **2022**, *12*, 2860. [[CrossRef](#)] [[PubMed](#)]
44. Ravichandran, R.; Annamalai, K.; Annamalai, A.; Elumalai, S. Solid state—Green construction of starch- beaded Fe<sub>3</sub>O<sub>4</sub>@Ag nanocomposite as superior redox catalyst. *Colloids Surf. A Physicochem. Eng. Asp.* **2023**, *664*, 131117. [[CrossRef](#)]
45. Iranzad, F.; Gheibi, M.; Eftekhari, M. Synthesis and application of polythiophene-coated Fe<sub>3</sub>O<sub>4</sub> nanoparticles for preconcentration of ultra-trace levels of cadmium in different real samples followed by electrothermal atomic absorption spectrometry. *Int. J. Environ. Anal. Chem.* **2018**, *98*, 16–30. [[CrossRef](#)]
46. Wojtysiak, S.; Kudelski, A. Influence of oxygen on the process of formation of silver nanoparticles during citrate/borohydride synthesis of silver sols. *Colloids Surf. A Physicochem. Eng. Asp.* **2012**, *410*, 45–51. [[CrossRef](#)]
47. Song, Y.; Chen, J.; Yang, X.; Zhang, D.; Zou, Y.; Ni, D.; Ye, J.; Yu, Z.; Chen, Q.; Jin, S.; et al. Fabrication of Fe<sub>3</sub>O<sub>4</sub>@Ag magnetic nanoparticles for highly active SERS enhancement and paraquat detection. *Microchem. J.* **2022**, *173*, 107019. [[CrossRef](#)]
48. Johnson, P.; Christy, R. Optical constants of the noble metals. *Phys. Rev. B* **1972**, *6*, 4370–4379. [[CrossRef](#)]
49. Iqbal, M.; Usanase, G.; Oulmi, K.; Aberkane, F.; Bendaikha, T.; Fessi, H.; Zine, N.; Agusti, G.; Errachid, E.; Elaissari, A. Preparation of gold nanoparticles and determination of their particles size via different methods. *Mater. Res. Bull.* **2016**, *79*, 97–104. [[CrossRef](#)]
50. Zulikifli, F.W.A.; Yazid, H.; Halim, M.Z.B.A.; Jani, A.M.M. Synthesis of gold nanoparticles on multi-walled carbon nanotubes (Au-MWCNTs) via deposition precipitation method. *AIP Conf. Proc.* **2017**, *1877*, 070003.
51. Acharya, D.; Mohanta, B.; Pandey, P.; Singha, M.; Nasiri, F. Optical and antibacterial properties of synthesised silver nanoparticles. *Micro Nano Lett.* **2017**, *12*, 223–226. [[CrossRef](#)]
52. Boussif, O.; Lezoualc’h, F.; Zanta, M.A.; Mergny, M.D.; Scherman, D.; Demeneix, B.; Behr, J.P. A versatile vector for gene and oligonucleotide transfer into cells in culture and in vivo: Polyethylenimine. *Proc. Natl. Acad. Sci. USA* **1995**, *92*, 7297–7301. [[CrossRef](#)] [[PubMed](#)]
53. Salihov, S.V.; Ivanenkov, Y.A.; Krechetov, S.P.; Veselov, M.S.; Sviridenkova, N.V.; Savchenko, A.G.; Klyachko, N.L.; Golovin, Y.I.; Chufarova, N.V.; Beloglazkina, E.K.; et al. Recent advances in the synthesis of Fe<sub>3</sub>O<sub>4</sub>@Au core/shell nanoparticles. *J. Magn. Magn. Mater.* **2015**, *394*, 173–178. [[CrossRef](#)]
54. Xing, Y.; Jin, Y.Y.; Si, J.C.; Peng, M.L.; Wang, X.F.; Chen, C.; Cui, Y.L. Controllable synthesis and characterization of Fe<sub>3</sub>O<sub>4</sub>/Au composite nanoparticles. *J. Magn. Magn. Mater.* **2015**, *380*, 150–156. [[CrossRef](#)]
55. Gerulová, K.; Kucmanová, A.; Sanny, Z.; Garaiová, Z.; Seiler, E.; Čaplovičová, M.; Čaplovič, L.; Palcut, M. Fe<sub>3</sub>O<sub>4</sub>-PEI Nanocomposites for Magnetic Harvesting of *Chlorella vulgaris*, *Chlorella ellipsoidea*, *Microcystis aeruginosa*, and *Auxenochlorella protothecoides*. *Nanomaterials* **2022**, *12*, 1786. [[CrossRef](#)] [[PubMed](#)]
56. Félix, L.; Martínez, M.A.R.; Salazar, D.G.P.; Coaquira, J.A.H. One-step synthesis of polyethyleneimine-coated magnetite nanoparticles and their structural, magnetic, and power absorption study. *RSC Adv.* **2020**, *10*, 41807–41815. [[CrossRef](#)]
57. Liang, R.; Yao, G.; Fan, L.; Qiu, J. Magnetic Fe<sub>3</sub>O<sub>4</sub>@Au composite-enhanced surface plasmon resonance for ultrasensitive detection of magnetic nanoparticle-enriched  $\alpha$ -fetoprotein. *Anal. Chim. Acta* **2012**, *737*, 22–28. [[CrossRef](#)] [[PubMed](#)]
58. Ilawe, N.V.; Oviedo, M.B.; Wong, B.M. Effect of quantum tunneling on the efficiency of excitation energy transfer in plasmonic nanoparticle chain waveguides. *J. Mater. Chem. C* **2018**, *6*, 5857–5864. [[CrossRef](#)]
59. Terrés-Haro, J.M.; Monreal-Trigo, J.; Hernández-Montoto, A.; Ibáñez-Civera, F.J.; Masot-Peris, R.; Martínez-Máñez, R. Finite Element Models of Gold Nanoparticles and Their Suspensions for Photothermal Effect Calculation. *Bioengineering* **2023**, *10*, 232. [[CrossRef](#)]
60. Lin, C.; Zhu, G.; Liu, G.; Zhu, L. FDTD simulation of the optical properties for gold nanoparticles. *Mater. Res. Express* **2020**, *7*, 125009.
61. Chu, D.T.; Sai, D.C.; Luu, Q.M.; Tran, H.T.; Quach, T.D.; Kim, D.H.; Nguyen, N.H. Synthesis of Bifunctional Fe<sub>3</sub>O<sub>4</sub>@SiO<sub>2</sub>-Ag Magnetic-Plasmonic Nanoparticles by an Ultrasound Assisted Chemical Method. *J. Electron. Mater.* **2017**, *46*, 3646–3653. [[CrossRef](#)]

**Disclaimer/Publisher’s Note:** The statements, opinions and data contained in all publications are solely those of the individual author(s) and contributor(s) and not of MDPI and/or the editor(s). MDPI and/or the editor(s) disclaim responsibility for any injury to people or property resulting from any ideas, methods, instructions or products referred to in the content.